10

The γ_{eff} Approach and Approximate Relations for the Determination of Aerothermodynamic Parameters

In this book, we employ approximate relations for the determination of aerothermodynamic data. These are used in order to give quantitative information and to illustrate phenomena. In order to be sufficiently self-consistent, we provide these relations as well as others here. Derived are first elements of the RHPM$^+$ flyer and the γ_{eff} approach together with the bow shock total pressure loss. Some γ_{eff} results in the large Mach number limit are given. Then the used or referred-to relations for the estimation of transport properties are provided, and finally formulas for stagnation point heating and flat surface boundary layer parameters. References are provided in all instances. For more general and detailed information the reader is referred to [1].

10.1 Elements of the RHPM$^+$ Flyer: γ_{eff} Approach and Bow Shock Total Pressure Loss

10.1.1 Introduction and Delineation

In [1], the RHPM[1] flyer was introduced, which can be used to illustrate, quantitatively with care and to a certain degree, characteristic aerothermodynamic properties of the different vehicle classes. It is essentially a two-dimensional approximation of the sufficiently flat windward side of the vehicle[2] by a flat surface (neglecting the nose bluntness) or a succession of flat surfaces, if aerodynamic trim and/or control surfaces, or inlet ramps are considered. To this geometrical approximation, the shock/expansion theory is applied, therefore the name RHPM flyer. The RHPM flyer can be a fair or a rather crude approximation of real flight vehicles, depending on the geometry under consideration. The more slender a configuration is and the smaller the angle of attack, the better is the approximation, for example, the wall pressure coefficient c_{p_w}. Flow properties influenced by the fact that a blunt nose is present in reality and therefore a total pressure loss is incurred, for example flow velocity and

---

[1]   RHPM stands for Rankine–Hugoniot–Prandtl–Meyer.
[2]   This means, that the angle of attack of the RHPM flyer is not necessarily the nominal angle of attack α of the approximated vehicle, but the inclination angle $\overline{\alpha}$, eq. (4.4), or a suitable mean angle.

Mach number at the body surface, may show larger errors. This holds also if high temperature real gas effects are present in reality. All should be checked beforehand for the case considered.

If more exact data are needed, simplified configurations can be employed, which approximate the lower symmetry line of, for instance, a RV-W. Examples are the asymptotic half-angle hyperboloid approximating the windward centerline of the Space Shuttle Orbiter [2], and the hyperboloid-flare approximation of the windward centerline with bodyflap deflection of the HERMES vehicle [3]. Of course, simple estimates are no more possible for these axisymmetric configurations, since solutions of the Euler or Navier–Stokes equations must be performed.

In Chapter 3, we use a sphere-cone (blunt cone) approximation for the windward symmetry line of the Space Shuttle Orbiter. We must accept the curvature jump at the sphere/cone junction, but obtain better asymptotic data for the flat part of the vehicle than with the asymptotic half-angle hyperboloid approximation. The nose radius is a function of the angle of attack [2, 4].

We give now elements of an extension of the original RHPM flyer to the RHPM$^+$ flyer, taking into account a) a γ_{eff} for the flow past the vehicle including the bow shock,[3] different from γ_∞, Sub-Sections 10.1.2 to 10.1.4, and b) the influence of the total pressure loss due to the vehicle's bow shock, approximated via the flow-normal portion of the bow shock, Sub-Section 10.1.5. While using the RHPM$^+$ flyer approximation we must be aware of the limitations discussed above. Especially we must note that the error due to the basic RHPM approximation can be larger than that we get without taking into account high temperature real gas effects. Nevertheless, in suitable cases we are able to quantify approximately the latter, at least parametrically.

10.1.2 The γ_{eff} Approach: General Considerations

The use of an effective ratio of the specific heats γ_{eff} permits high temperature real gas effects to be accounted for approximately. For example, for the Space Shuttle Orbiter at $M_\infty = 24$ and $\alpha = 40°$, ratios of specific heats computed numerically are $\gamma \approx 1.3$ just behind the bow shock in the nose region, $\gamma \approx 1.12$ close to the body in the nose region and $\gamma \approx 1.14$ along the lower body surface [5]. Although aerothermodynamic parameters found with approximate methods (shock–expansion theory, Newton-derived methods) employing the γ_{eff} approach must be considered with care, such methods can be used to quantify, parameterize, and illustrate real-gas effects in a simple way.

Approximate methods need first of all the relations for flow parameter changes across a shock wave. The shock relations usually found in the literature are derived for a constant ratio of specific heats ($\gamma = $ const.) in the whole flow domain considered (nominal case). If we wish to consider high temperature real gas effects in approximate flow field relations for a flight vehicle, we

---

[3] γ_{eff} of course must be either be known beforehand from other sources, or is applied parametrically.

have ahead of the vehicle the original atmosphere with $\gamma = \gamma_\infty$ ($= 1.4$ for air). If we chose an effective ratio of specific heats $\gamma_{eff} < \gamma_\infty$, which then is constant behind the shock wave and on the body surface, we have two different ratios of specific heats in the whole flow domain.

In the situation posed above, the shock relations are different from those for the nominal case found in the literature, e.g., [6]. Of course, the conservation of mass, momentum and enthalpy across a shock wave must be fulfilled also here. We show first the detailed derivation of the relations for the normal shock wave and give then the relations for the oblique shock wave. Unfortunately for the γ_{eff} approach compact-form relations as those given in [6] are no more achievable. We use the classical approach with '1' designating the parameters ahead of the shock wave, and '2' those behind it (in applications '1' would denote the parameters ahead of the shock with γ_∞, and '2' the parameters behind the shock with γ_{eff}). The familiar pressure coefficient c_{p_2} reads

$$c_{p_2} = \frac{p_2 - p_1}{q_1} = \frac{2}{\gamma_1 M_1^2}\left(\frac{p_2}{p_1}|_{\gamma_2} - 1\right) = \frac{2}{\gamma_\infty M_\infty^2}\left(\frac{p_2}{p_\infty}|_{\gamma_{eff}} - 1\right). \qquad (10.1)$$

10.1.3 Normal Shock Wave

For a normal shock wave, the equations for the conservation of the three entities read, with h_t being the total enthalpy:

$$\rho_1 v_1 = \rho_2 v_2, \qquad (10.2)$$

$$\rho_1 v_1^2 + p_1 = \rho_2 v_2^2 + p_2, \qquad (10.3)$$

$$(h_{t_1} =)\ \ h_1 + \frac{1}{2}v_1^2 = h_2 + \frac{1}{2}v_2^2\ \ (= h_{t_2}). \qquad (10.4)$$

In the γ_{eff} approach, the latter relation is changed. Noting that c_{p_1} and c_{p_2} denote here the specific heats at constant pressure:

$$h_1 = c_{p_1}T_1 = \frac{\gamma_1}{\gamma_1 - 1}R_1 T_1 = \frac{\gamma_1}{\gamma_1 - 1}\frac{p_1}{\rho_1}, \qquad (10.5)$$

and

$$h_2 = c_{p_2}T_2 = \frac{\gamma_2}{\gamma_2 - 1}R_2 T_2 = \frac{\gamma_2}{\gamma_2 - 1}\frac{p_2}{\rho_2}. \qquad (10.6)$$

We obtain instead of eq. (10.4)

$$(h_{t_1} =)\ \ \frac{\gamma_1}{\gamma_1 - 1}\frac{p_1}{\rho_1} + \frac{1}{2}v_1^2 = \frac{\gamma_2}{\gamma_2 - 1}\frac{p_2}{\rho_2} + \frac{1}{2}v_2^2\ \ (= h_{t_2}). \qquad (10.7)$$

Note that $p_1 = \rho_1 T_1 R_1$ and $p_2 = \rho_2 T_2 R_2$. Because we connect the thermodynamic entities ahead '1' and behind '2' the shock analytically, we must also connect the specific gas constants R_1 and R_2 with each other [7]. This is made with the so called compressibility factor $Z = Z(\rho, T)$

$$R_2 = Z(\rho_2, T_2)R_1. \tag{10.8}$$

The compressibility factor in the frame of our considerations is, in the few cases where needed, a problematic issue. Details are given in Sub-Section 10.1.6.

In the classical way, it follows then from eqs. (10.2) and (10.3)

$$v_1^2 = \left(\frac{\rho_2}{\rho_1}\right)\frac{p_2 - p_1}{\rho_2 - \rho_1}, \tag{10.9}$$

and

$$v_2^2 = \left(\frac{\rho_1}{\rho_2}\right)\frac{p_2 - p_1}{\rho_2 - \rho_1}, \tag{10.10}$$

and finally

$$v_2^2 = \left(\frac{\rho_1}{\rho_2}\right)^2 v_1^2. \tag{10.11}$$

Putting eqs. (10.9) and (10.10) into eq. (10.7), we obtain the so-called Hugoniot relation which combines the thermodynamic parameters ahead and behind the shock wave

$$h_2 - h_1 = \frac{\gamma_2}{\gamma_2 - 1}\frac{p_2}{\rho_2} - \frac{\gamma_1}{\gamma_1 - 1}\frac{p_1}{\rho_1} = \frac{1}{2}\left(\frac{1}{\rho_1} + \frac{1}{\rho_2}\right)(p_2 - p_1). \tag{10.12}$$

From this the pressure ratio across the shock wave is obtained

$$\frac{p_2}{p_1} = \left(\frac{\gamma_2 - 1}{\gamma_1 - 1}\right)\frac{\frac{\rho_2}{\rho_1}(\gamma_1 + 1) - (\gamma_1 - 1)}{(\gamma_2 + 1) - \frac{\rho_2}{\rho_1}(\gamma_2 - 1)}. \tag{10.13}$$

The Mach number M_1 and speed of sound a_1 are defined by

$$M_1 = \frac{v_1}{a_1}, \tag{10.14}$$

$$a_1 = \sqrt{\gamma_1 R_1 T_1} = \sqrt{\gamma_1 \frac{p_1}{\rho_1}}. \tag{10.15}$$

Combining eq. (10.14) with eq. (10.9) yields the connection of the pressure and the density ratio across the shock with the Mach number M_1 ahead of it

$$\frac{1}{\gamma_1}\left(\frac{\rho_2}{\rho_1}\right)\frac{p_2/p_1 - 1}{\rho_2/\rho_1 - 1} = M_1^2. \tag{10.16}$$

We substitute here p_2/p_1 with eq. (10.13) and obtain the relation for the density ratio

$$\left(\frac{\rho_2}{\rho_1}\right)^2\left[\gamma_1 M_1^2(\gamma_2 - 1) + 2\gamma_1\frac{\gamma_2 - 1}{\gamma_1 - 1}\right] +$$
$$+ \left(\frac{\rho_2}{\rho_1}\right)\left[-2\gamma_1 M_1^2\gamma_2 - 2\gamma_2\right] + \left[\gamma_1 M_1^2(\gamma_2 + 1)\right] = 0. \tag{10.17}$$

If we denote the terms in the three square brackets with A, B, and C, respectively, we get a solution with

$$\left.\frac{\rho_2}{\rho_1}\right|_{1,2} = \frac{-B \pm \sqrt{B^2 - 4AC}}{2A} \quad \left(= \left.\frac{v_1}{v_2}\right|_{1,2}\right). \tag{10.18}$$

A compact-form solution as for a constant γ in the whole flow domain [1, 6] is not possible. The positive sign of the square root is valid. The result is then used to determine numerically the other ratios across the shock wave (see below). Choosing $\gamma_2 \equiv \gamma_1 = \gamma$ yields the familiar compact-form solutions for this and all other parameter ratios. If $\gamma_1 \neq \gamma_2$, the case $M_1 = 1$ is not included, because we assume isenthalpic flow.

For $M_1 \rightarrow \infty$ we get further

$$\left.\frac{\rho_2}{\rho_1}\right|_{M_1 \rightarrow \infty} = \frac{\gamma_2 + 1}{\gamma_2 - 1}, \tag{10.19}$$

and also the other limiting cases, given for instance in [1].

The temperature ratio T_2/T_1 is determined from:

$$\frac{T_2}{T_1} = \frac{p_2}{p_1} \frac{\rho_1}{\rho_2} \frac{R_1}{R_2}. \tag{10.20}$$

The speed of sound behind the shock a_2 is defined by:

$$a_2 = \sqrt{\gamma_2 T_2 R_2} = \sqrt{\gamma_2 p_2/\rho_2}. \tag{10.21}$$

The Mach number $M_2 = v_2/a_2$ is found with the help of eqs. (10.11) and (10.21) after some manipulation in the following way:

$$M_2^2 = \frac{v_2^2}{a_2^2} = \left(\frac{\rho_1}{\rho_2}\right)^2 v_1^2 \frac{\rho_2}{\gamma_2 p_2} = \frac{\gamma_1}{\gamma_2} M_1^2 \frac{\rho_1}{\rho_2} \frac{p_1}{p_2}. \tag{10.22}$$

It remains to determine the total pressure p_{t_2}, total density ρ_{t_2} and total temperature[4] T_{t_2} behind the shock wave. The total pressure p_{t_2} is found from

$$\frac{p_{t_2}}{p_{t_1}} = \frac{p_{t_2}}{p_2} \frac{p_2}{p_1} \frac{p_1}{p_{t_1}}, \tag{10.23}$$

with p_2/p_1 from eq. (10.13) after solution of eq (10.17), and

$$\frac{p_{t_2}}{p_2} = \left(1 + \frac{\gamma_2 - 1}{2} M_2^2\right)^{\gamma_2/(\gamma_2 - 1)}, \quad \frac{p_{t_1}}{p_1} = \left(1 + \frac{\gamma_1 - 1}{2} M_1^2\right)^{\gamma_1/(\gamma_1 - 1)}. \tag{10.24}$$

---

[4] The total enthalpy is constant, but the total temperature is not because of eq. (10.7).

Table 10.1. Flow parameters ratios across a normal shockwave with γ_{eff}, and the equations and the input for their numerical determination.

Parameter Ratio	Symbol	Eq.	Input
Density	ρ_2/ρ_1	(10.17)	$\gamma_1, \gamma_2, M_1^2$
Pressure	p_2/p_1	(10.13)	$\gamma_1, \gamma_2, \rho_2/\rho_1$
Temperature	T_2/T_1	(10.20)	$p_2/p_1, \rho_2/\rho_1, R_2$
Velocity	v_2/v_1	(10.2)	ρ_2/ρ_1
Mach number	M_2/M_1	(10.22)	$\gamma_1, \gamma_2, \rho_2/\rho_1, p_2/p_1$
Total pressure	p_{t_2}/p_{t_1}	(10.23)	$p_{t_2}/p_1, p_2/p_1, p_{t_1}/p_1$
Total density	ρ_{t_2}/ρ_{t_1}	(10.25)	$\rho_{t_2}/\rho_1, \rho_2/\rho_1, \rho_{t_1}/\rho_1$
Total temperature	T_{t_2}/T_{t_1}	(10.27)	$p_{t_2}/p_{t_1}, \rho_{t_2}/\rho_{t_1}, R_2$

Similarly we find for the total density ρ_{t_2}:

$$\frac{\rho_{t_2}}{\rho_{t_1}} = \frac{\rho_{t_2}}{\rho_2} \frac{\rho_2}{\rho_1} \frac{\rho_1}{\rho_{t_1}}, \tag{10.25}$$

with

$$\frac{\rho_{t_2}}{\rho_2} = \left(1 + \frac{\gamma_2 - 1}{2} M_2^2\right)^{1/(\gamma_2-1)} \quad, \quad \frac{\rho_{t_1}}{\rho_1} = \left(1 + \frac{\gamma_1 - 1}{2} M_1^1\right)^{1/(\gamma_1-1)}. \tag{10.26}$$

The total temperature T_{t_2} is to be determined with

$$\frac{T_{t_2}}{T_{t_1}} = \frac{p_{t_2}}{p_{t_1}} \frac{\rho_{t_1}}{\rho_{t_2}} \frac{R_1}{R_2}, \tag{10.27}$$

or directly with the help of eq. (10.4), respectively eq. (10.7):

$$T_{t_2} = \frac{\gamma_2 - 1}{\gamma_2} \frac{1}{R_2} \left(\frac{\gamma_2}{\gamma_2 - 1} \frac{p_2}{\rho_2} + \frac{1}{2} v_2^2\right). \tag{10.28}$$

Looking back, we observe, that the gas constant behind the shock wave R_2 is needed only if we want to determine the temperatures T_2 and/or T_{t_2}. This is a restriction which we cannot overcome with an adequately simple approximation of the compressibility factor $Z(\rho, T) = Z(\gamma_{eff})$, Sub-Section 10.1.6. Because we do not get a compact-form solution for ρ_2/ρ_1, we also do not have such solutions for the other parameter ratios. We note in Table 10.1 the input into the respective equations for the numerical determination of these ratios, for the temperatures with the caveat in view of the compressibility factor.
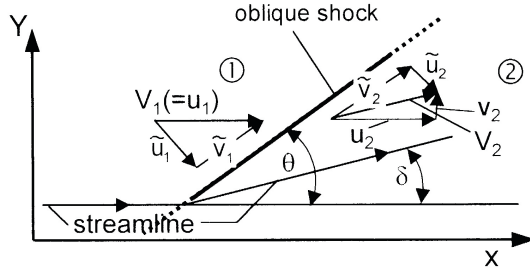
Fig. 10.1. Schematic of an oblique shock wave and notation [1].

10.1.4 Oblique Shock Wave

For the oblique shock wave, Fig. 10.1, the equations for the conservation of the three entities mass, momentum (now two components: normal and tangential to the oblique shock wave), and enthalpy read

– mass

$$\rho_1 \tilde{u}_1 = \rho_2 \tilde{u}_2, \tag{10.29}$$

– normal momentum component

$$\rho_1 \tilde{u}_1^2 + p_1 = \rho_2 \tilde{u}_2^2 + p_2, \tag{10.30}$$

– tangential momentum component

$$\rho_1 \tilde{u}_1 \tilde{v}_1 = \rho_2 \tilde{u}_2 \tilde{v}_2, \tag{10.31}$$

– enthalpy

$$(h_{t_1} =) \ h_1 + \frac{1}{2}(\tilde{u}_1^2 + \tilde{v}_1^2) = h_2 + \frac{1}{2}(\tilde{u}_2^2 + \tilde{v}_2^2) \ (= h_{t_2}). \tag{10.32}$$

We note especially that the resultant velocity behind the shock wave V_2 is related to that ahead of it V_1 by

$$V_2^2 = V_1^2 \left[\left(\frac{\rho_1}{\rho_2} \right)^2 \sin^2 \theta + \cos^2 \theta \right]. \tag{10.33}$$

We proceed as before and find the Hugoniot relation in the same form

$$h_2 - h_1 = \frac{\gamma_2}{\gamma_2 - 1} \frac{p_2}{\rho_2} - \frac{\gamma_1}{\gamma_1 - 1} \frac{p_1}{\rho_1} = \frac{1}{2} \left(\frac{1}{\rho_1} + \frac{1}{\rho_2} \right) (p_2 - p_1). \tag{10.34}$$

Now, however, the relevant Mach number is that of the flow component normal to the shock wave

$$\tilde{M}_1 = \sin \theta \, M_1 = \frac{\tilde{u}_1}{a_1}. \tag{10.35}$$

Proceeding further as for the normal shock wave, we obtain:

$$\frac{1}{\gamma_1}\left(\frac{\rho_2}{\rho_1}\right)\frac{(p_2/p_1)-1}{(\rho_2/\rho_1)-1} = \tilde{M}_1^2 = \sin^2\theta\, M_1^2.$$
(10.36)

The temperature T_2 again is

$$\frac{T_2}{T_1} = \frac{p_2}{p_1}\frac{\rho_1}{\rho_2}\frac{R_1}{R_2}.$$
(10.37)

and the speed of sound behind the shock wave

$$a_2 = \sqrt{\gamma_2 T_2 R_2} = \sqrt{\gamma_2 p_2/\rho_2}.$$
(10.38)

The Mach number $M_2 = v_2/a_2$ now is found with the help of eqs. (10.33) and (10.38) to be

$$M_2^2 = \frac{V_2^2}{a_2^2} = \left(\frac{\rho_1}{\rho_2}\right)^2 V_1^2 \frac{\rho_2}{\gamma_2 p_2} = \frac{\gamma_1}{\gamma_2}M_1^2\left[\left(\frac{\rho_1}{\rho_2}\right)^2\sin^2\theta + \cos^2\theta\right]\frac{\rho_2}{\rho_1}\frac{p_1}{p_2}.$$
(10.39)

The shock angle θ is an unknown. From Fig. 10.1 we find, with

$$\tan\theta = \frac{\tilde{u}_1}{\tilde{v}_1}, \quad \tan(\theta-\delta) = \frac{\tilde{u}_2}{\tilde{v}_2},$$
(10.40)

and eq. (10.29) the relation

$$\frac{\tan\theta}{\tan(\theta-\delta)} = \frac{\tilde{u}_1}{\tilde{v}_1}\frac{\tilde{v}_2}{\tilde{u}_2} = \frac{\tilde{u}_1}{\tilde{u}_2} = \frac{\rho_2}{\rho_1}.$$
(10.41)

After some manipulation with eqs. (10.34), (10.36) and (10.41) as for the normal shock wave, we obtain two coupled equations for the two unknowns ρ_2/ρ_1 and $\tan\theta$ as functions of the free-stream Mach number M_1, the deflection angle δ, and the two ratios of specific heats γ_1 and γ_2:

$$\left(\frac{\rho_2}{\rho_1}\right)^2\left[\gamma_1\sin^2\theta\, M_1^2(\gamma_2-1) + 2\gamma_1\frac{\gamma_2-1}{\gamma_1-1}\right] +$$
$$+ \left(\frac{\rho_2}{\rho_1}\right)\left[-2\gamma_1\sin^2\theta\, M_1^2\gamma_2 - 2\gamma_2\right] + \left[\gamma_1\sin^2\theta\, M_1^2(\gamma_2+1)\right] = 0,$$
(10.42)

and

$$\tan^2\theta\,[\tan\delta] + \tan\theta\left[1 - \frac{\rho_2}{\rho_1}\right] + \left[\frac{\rho_2}{\rho_1}\tan\delta\right] = 0.$$
(10.43)

The latter equation written in the form

$$\tan\delta = \frac{(\rho_2/\rho_1)-1}{(\rho_2/\rho_1)+\tan^2\theta}\tan\theta$$
(10.44)

leads for $\gamma_2 \equiv \gamma_1 = \gamma$ to the familiar compact-form relation for $\tan \delta$. The case $\gamma_1 \neq \gamma_2$ for $\delta = 0°$ is not included, again because we assume isenthalpic flow.

We proceed further and find the pressure p_2 like for the normal shock with the help of:

$$\frac{p_2}{p_1} = \left(\frac{\gamma_2 - 1}{\gamma_1 - 1} \right) \frac{(\rho_2/\rho_1)(\gamma_1 + 1) - (\gamma_1 - 1)}{(\gamma_2 + 1) - (\rho_2/\rho_1)(\gamma_2 - 1)}. \tag{10.45}$$

The velocity components normal to and behind the shock wave read:

$$\tilde{u}_2 = \frac{\rho_1}{\rho_2} V_1 \sin \theta, \tag{10.46}$$

and, because of eq. (10.31),

$$\tilde{v}_1 = \tilde{v}_2 = V_1 \cos \theta. \tag{10.47}$$

The resultant velocity behind the shock wave, Fig. 10.1, is:

$$V_2 = \sqrt{\tilde{u}_2^2 + \tilde{v}_2^2}. \tag{10.48}$$

Total pressure p_{t_2}, total density ρ_{t_2} and total temperature T_{t_2} can be found like for the normal shock wave. Again we need the specific gas constant R_2, if we wish to determine T_2 and/or T_{t_2}.

For the numerical determination of all parameters a scheme similar to that given in Table 10.1 can be devised, which however has to include eq. (10.43) for θ.

10.1.5 Bow Shock Total Pressure Loss: Restitution of Parameters of a One-Dimensional Surface Flow

With extended algebraic effort it can be shown that the governing equations for inviscid fluid flow around a body can be reduced exactly from their three-dimensional or two-dimensional form *off* the body surface, of course, including the surface, to the two-dimensional or one-dimensional form only *on* the surface. We take this for granted and consider now, how for a two-dimensional body from a given pressure distribution along the surface other flow parameters can be determined, while taking into account the total pressure loss due to the flow-normal portion of the bow shock. This is of interest, if for instance with Newton's method the pressure on the surface of a body was found, if a consideration like in Sub-Section 6.1.1 is made, or if experimental pressure data are given, and further investigations are intended.

We have to make one assumption, viz., that the streamline hitting the forward stagnation point crossed the locally normal bow shock surface [1]. Usually at large angles of attack this is not the case, but in general it is an acceptable assumption. With this assumption, we can obtain,[5] with $\gamma_{eff} = \gamma_2 = \text{const.}$,

---

[5]   We give, despite the problems with the compressibility factor, the derivation in terms of γ_{eff}.

the total pressure p_{t_2} and the total density ρ_{t_2} at the forward stagnation point on the body surface from eqs. (10.23) and (10.25). Both are constant along the body surface as long as we can assume that no embedded shock waves are present there.

Starting at the stagnation point, we denote the coordinate along the surface with x. If total pressure, total density, and the pressure $p(x)$ are given, we find with the help of Bernoulli's equation the velocity $v_2(x)$:

$$v_2(x) = \sqrt{\frac{2\gamma_2}{\gamma_2 - 1}\frac{p_{t_2}}{\rho_{t_2}}\left[1 - \left(\frac{p_2(x)}{p_{t_2}}\right)^{(\gamma_2-1)/\gamma_2}\right]}. \qquad (10.49)$$

Taking into account constant total enthalpy $h_{t_2} = h_{t_1}$, the temperature $T(x)$ is determined from

$$h_2(x) = h_{t_1} - \frac{1}{2}v_2^2(x), \qquad (10.50)$$

and

$$T_2(x) = \frac{h_2(x)}{c_{p_2}} = \frac{\gamma_2 - 1}{\gamma_2}\frac{1}{R_2}h_2(x). \qquad (10.51)$$

From this follows the Mach number $M_2(x)$

$$M_2(x) = \frac{v_2(x)}{\sqrt{\gamma_2 R_2 T_2(x)}}, \qquad (10.52)$$

and finally the density $\rho_2(x)$ with

$$\rho_2(x) = \frac{p_2(x)}{R_2 T_2(x)}, \qquad (10.53)$$

and, for checking purposes

$$\rho_2(x) = \rho_{t_2}\left[1 + \frac{\gamma_2 - 1}{2}M_2^2(x)\right]^{-1/(\gamma_2-1)}. \qquad (10.54)$$

The specific gas constant $R_2 = Z R_1$, appears quite often in these relations. This means that the compressibility factor plays a larger role here, than in the shock relations. In general it can not be recommended to use the γ_{eff} approach for the restitution of flow parameters, as described here, unless an exact numerical reference solution for a given problem permits to develop a simple approximation of Z valid for this problem, see the next sub-section.

10.1.6 The Compressibility Factor Z

Consider a mixture of n thermally perfect gases. The equation of state, with the universal gas constant R_0 is [1]:

$$p = \sum_{i=1}^{n} p_i = \sum_{i=1}^{n} \rho_i \frac{R_0}{M_i} T = \rho T \sum_{i=1}^{n} c_i \frac{R_0}{M_i} = \rho T R, \qquad (10.55)$$

with p_i being the partial pressure, ρ_i the partial density, M_i the mass of the species i, R the gas constant of the mixture. The mass fraction[6] c_i ($0 \leqq c_i \leqq 1$) of the species i is

$$c_i = \frac{\rho_i}{\rho}, \qquad (10.56)$$

and the mean molecular weight M is given by

$$\frac{1}{M} = \sum_{i=1}^{n} \frac{c_i}{M_i}. \qquad (10.57)$$

If we consider a single diatomic gas, for instance N_2, it is obvious that the specific gas constant R is twice as large for the fully dissociated gas ($c_{N_2} = 0$) than for the undissociated gas ($c_{N_2} = 1$). If we express the specific gas constant in the dissociated state with R_2, it is related to that of the undissociated gas R_1 by

$$R_2 = Z(\rho, T) R_1 \qquad (10.58)$$

where Z is the compressibility factor [7]. It is found with eqs. (10.55) and (10.57):

$$Z = \frac{R_2}{R_1} = \frac{\sum_{i=1}^{n} c_i R_0 / M_i|_2}{\sum_{i=1}^{n} c_i R_0 / M_i|_1} = \frac{M_1}{M_2}. \qquad (10.59)$$

For air in equilibrium in the temperature range $1{,}500\,K \leqq T \leqq 15{,}000\,K$ and the density range $1 \leqq \log_{10}(\rho/\rho_0) \leqq -10$, with $\rho_0 = 1.293 \cdot 10^{-3}\,\mathrm{g/cm^3}$ a graph is given in [7] which shows a highly nonlinear behavior of $Z(\rho, T)$, with $1 \leqq Z \lessapprox 4$. For $\log_{10}(\rho/\rho_0) = -5$, for instance, the compressibility factor is $Z \approx 1.3$, 2 and 3.2 for $T = 4{,}000, 6{,}000$ and $10{,}000$ K respectively. We expressly state that all this is no problem in discrete numerical solutions of the governing equations of aerothermodynamics, where we do not need these data beforehand in the computation process, but can construct for instance Z or γ_{eff} a posteriori.

If we employ γ_{eff} in analytical methods of the kinds presented here, however, we need for the determination of some thermodynamic and flow entities the compressibility factor Z, which means—note that this is the critical point—its connection with γ_{eff}: $Z = Z(\gamma_{eff})$. An expression of $Z = Z(\gamma_{eff})$ is not known. It is advisable, therefore, to use the γ_{eff} approach only for the determination of data where Z does not play a role. Across shock waves, these are almost all flow parameters with the exception of the temperatures T and T_t.

For the restitution of parameters of one-dimensional or other flows, one can try approximations of the kind $Z = a + b\,\gamma_{eff}$. This is permissible, if it can be shown with an exact numerical reference solution that this approximation is meaningful. Clearly then this approximation can only be employed in the class of problems to which the selected problem belongs.

---

[6] We use c_i as symbol instead of ω_i [1].

10.1.7 Results across Shocks in the Large M_1 Limit Using γ_{eff}

For the normal shock we have found, eq. (10.19), that ρ_2/ρ_1 in the limit, $M_1 \Rightarrow \infty$ depends on γ_2 only. This means that in that limit the state of the gas behind the shock wave does no more depend on the ratio of specific heats γ_1 ahead of the shock. We study this in more detail in Fig. 10.2.

The asymptotic behavior is seen well for ρ_2/ρ_1 and M_2. The limit is always reached later for smaller γ_1. From the ordinary Rankine–Hugoniot relations [1], we know that no large Mach number limits exist for p_2/p_1 and T_2/T_1. Hence we cannot assume that these properties become independent of γ_1 in the limit. This is also seen in the figure.

For the total pressure coefficient behind the shock wave $c_{p_{t2}}$, we see finally, Fig. 10.3, that it becomes independent of γ_1 for rather small M_1.

These results show on the one hand, that the γ_{eff} approach, which anyway must be handled with care, demands the use of the exact relations as we have derived them above. On the other hand, in certain cases, here for $c_{p_{t2}}$ in the range $M_1 \gtrsim 10$, it is permitted to plug into the Rankine–Hugoniot conditions, also for the oblique shock, just the value of γ_{eff} $(\equiv \gamma_2)$.
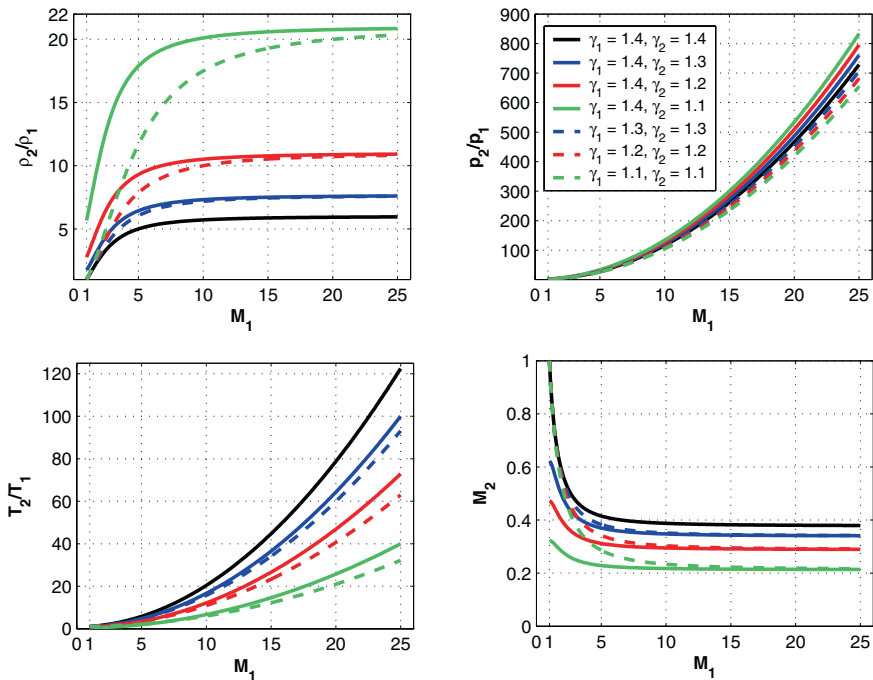
Fig. 10.2. Normal shock wave: dependence of density ratio (upper left), pressure ratio (upper right), temperature ratio (lower left) and Mach number behind the shock (lower right) on pairs of γ_1 and γ_2 as function of M_1.
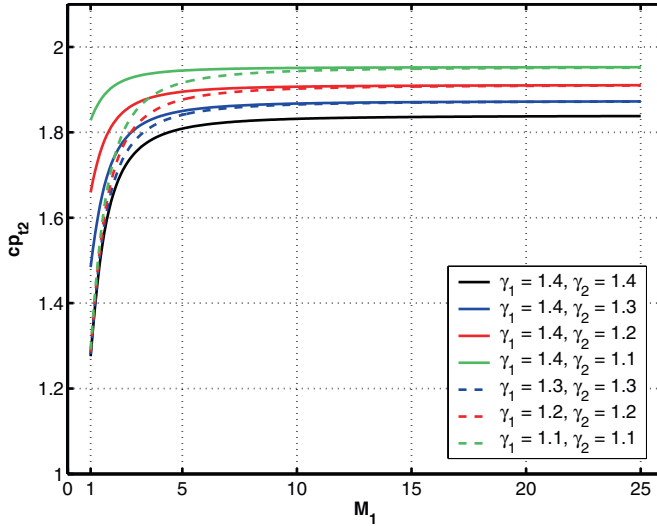
Fig. 10.3. Normal shock wave: dependence of the total pressure coefficient behind the shock wave $c_{p_{t2}}$ on pairs of γ_1 and γ_2 as function of M_1.

This means that a gas with a given γ_{eff} can be handled like a perfect gas by employing a constant γ ahead and behind the shock. This would be the justification to work in a ground simulation facility with gases other than air in order to study the influence of a chosen γ on the aerodynamic properties of a flight vehicle. An example is the investigation of the pitching moment anomaly of the Space Shuttle Orbiter, Section 3.5, in the LaRC 20" CF_4 (carbon tetrafluoride) tunnel [8].

10.2 Transport Properties

We list here only some power-law approximations for the viscosity and the thermal conductivity, valid for temperatures up to approximately 1,500–2,000 K. For details, see [1].

Air

– **Viscosity** (dimensions: μ [Pa s], T [K])

Sutherland's equation:

$$\mu = 1.458 \cdot 10^{-6} \frac{T^{1.5}}{T + 110.4}. \tag{10.60}$$

Simple power-law approximation:

$$\mu = c\,T^{\omega}, \tag{10.61}$$

where for $T \lesssim 200$ K: $c = 0.702 \cdot 10^{-7}$, $\omega = 1$; and for $T \gtrsim 200$ K: $c = 0.04644 \cdot 10^{-5}$, $\omega = 0.65$.

– **Thermal conductivity** (dimensions: k [W/(m K)], T [K], R_0 [J/(kg K)], c_p [J/(kg K)], M [kg])

The thermal conductivity of a molecular gas can be determined with the help of the Eucken formula, where c_p is the specific heat at constant pressure:

$$k = \left(c_p + \frac{5}{4}\frac{R_0}{M} \right) \mu. \tag{10.62}$$

The monatomic case is included, if for the specific heat $c_p = 2.5\,R_0/M$ is taken.

From the above the following relation the Prandtl number can be derived as function of the ratio of specific heats γ:

$$Pr = \frac{\mu c_p}{k} = \frac{c_p}{c_p + 1.25 R_0/M} = \frac{4\gamma}{9\gamma - 5}. \tag{10.63}$$

An explicit relations for air is the Hansen equation:

$$k = 1.993 \cdot 10^{-3}\frac{T^{1.5}}{T + 112.0}. \tag{10.64}$$

Simple power-law approximation:

$$k = c\,T^{\omega}, \tag{10.65}$$

where for $T \lesssim 200$ K: $c = 9.572 \cdot 10^{-5}$, $\omega = 1$; and for $T \gtrsim 200$ K: $c = 34.957 \cdot 10^{-5}$, $\omega = 0.75$.

Molecular Nitrogen

– **Viscosity** (dimensions like above)

Sutherland's equation for molecular nitrogen

$$\mu = 1.39 \cdot 10^{-6}\frac{T^{1.5}}{T + 102.0}. \tag{10.66}$$

– **Thermal conductivity** (dimensions like above)

The thermal conductivity of a molecular nitrogen can be determined, like for air, with the help of the Eucken formula, eq. (10.62).

10.3 Formulas for Stagnation Point Heating

At the early stages of aerothermodynamics there was nearly no possibility to measure or to theoretically determine the temperature gradient $\partial T/\partial y$ normal to the surface.[7] This temperature gradient determines by the Fourier law the convective heat-flux to an isothermal wall in a non-reacting flow, i.e., the heat flux in the gas at the wall [1]

$$q_{gw} = -k\frac{\partial T}{\partial y},\qquad(10.67)$$

where k is the thermal conductivity.[8]

Therefore, the so-called film formulation reads

$$q_{gw} = h_c(T_r - T_w),\qquad(10.68)$$

with T_r the recovery and T_w the wall temperature, and h_c the film coefficient. The latter is not a constant but depends on numerous variables, where the most important ones are the density and the velocity at the boundary layer edge as well as the transport properties. The film coefficient combines the effects of conduction and convection in the gas.

We list some of the most often used formulas for determining the stagnation point (sphere) heat-flux, which all are based on the film formulation concept, eq. (10.68). It is not the intention here to go in great detail, since applications of these formulas are numerously available in the literature. But we provide the reader with the possibility to have a first glance at the dependencies of forward stagnation point heat-fluxes for RV-W's and RV-NW's during atmospheric re-entry, but also CAV/ARV's. The SI basic and derived units, Section C.2, are employed.

a) Formula of Van Driest [9]

$$q_{gw} = k_{st}Pr^{-0.6}(\rho_e\mu_e)^{0.5}(h_r - h_w)_{st}\left(\frac{du_e}{dx}\right)_{st}^{0.5},\qquad(10.69)$$

with $k_{st} = 0.76$ for a sphere, Pr the Prandtl number, h_r the recovery enthalpy, h_w the fluid enthalpy at the wall, $du_e/dx|_{st}$ the tangential velocity gradient at the stagnation point, the subscript e denotes the boundary layer edge and st the stagnation point. Perfect gas is assumed. The velocity gradient $du_e/dx|_{st}$

---

[7]   With modern numerical simulation methods approximating the full Navier–Stokes equations including thermochemical non-equilibrium, this situation has changed and most of the gradients in the boundary layer can be resolved properly.

[8]   Note that usually for the wall heat flux the minus sign is omitted: $q_{gw} = k\,\partial T/\partial y$. If the y-coordinate is positive away from the surface, a heat flux towards the wall therefore has a positive value. This holds analogously also for the wall shear stress.

can be determined by Newton's pressure assumption at the stagnation point [1] or from Euler equations at the edge of the boundary layer using the relation:

$$\left(\frac{du_e}{dx}\right)_{st} = \frac{1}{R_N}\left(\frac{2(p_e - p_\infty)}{\rho_e}\right)^{0.5},\qquad(10.70)$$

with R_N being the nose radius.

b) Formula of Lees [10]

$$q_{gw} = 0.50Pr^{-0.67}(\rho_{st}\mu_{st})^{0.5}h_{w,st}\sqrt{2}\left(\frac{du_e}{dx}\right)_{st}^{0.5}.\qquad(10.71)$$

Perfect gas is assumed. This formula was used during the APOLLO project work for convective heat-flux prediction. For the heat-flux prediction away from the stagnation point on the APOLLO surface in the pitch plane the following relations were used exploiting the wall pressure distribution (e.g., known from wind tunnel experiment)

$$q_{gw} = 0.50Pr^{-0.67}(\rho_{st}\mu_{st})^{0.5}h_{w,st}F(s),\qquad(10.72)$$

$$F(s) = \frac{\dfrac{p_e}{p_{st}}\dfrac{\mu_e T_{st}}{\mu_{st}T_e}u_e r_o^k}{\left(2\displaystyle\int_o^{s1}\dfrac{p_e}{p_{st}}\dfrac{\mu_e T_{st}}{\mu_{st}T_e}u_e r_o^{2k}ds\right)^{0.5}},\qquad(10.73)$$

with $k = 1$ for axisymmetric flow and $k = 0$ for plane flow, s denotes the contour length measured from the stagnation point, r_0 the radius of the nose section of the body of revolution [11].

c) Formula of Fay and Riddell [12]

$$q_{gw} = 0.76Pr^{-0.6}(\rho_w\mu_w)^{0.1}(\rho_e\mu_e)^{0.4}\cdot$$
$$\cdot\left[1 + (Le^\phi - 1)\frac{h_D}{h_e}\right](h_e - h_w)_{st}\left(\frac{du_e}{dx}\right)_{st}^{0.5},\qquad(10.74)$$

with h_D being the enthalpy of dissociation of the gas mixture, $Le = Pr/Sc$ the Lewis number defining the ratio of heat transfer by mass diffusion to heat transfer by conduction [1]. For example, for dissociating air, the Prandtl number is $Pr = 0.71$ and the Schmidt number is $Sc = 0.5$, giving the Lewis number $Le = 1.42$; $Le = 0$ for frozen flow with non-catalytic wall, $\phi = 0.52$ for equilibrium flow and $\phi = 0.63$ for frozen flow with fully catalytic wall. This formula is likely the most often used and referenced relation for stagnation point heat-flux determination.

d) Formula of Cohen [13]

$$q_{gw} = 0.767 Pr^{-0.6}(\rho_w \mu_w)^{0.07}(\rho_e \mu_e)^{0.43}(h_e - h_w)_{st}\left(\frac{du_e}{dx}\right)_{st}^{0.5}. \qquad (10.75)$$

This equation is very similar to eq. (10.74) of Fay and Riddell for $Le = 0$ (frozen flow with non-catalytic wall) and is used in [14] as a basic relation in an engineering method for predicting the heat transfer at blunted cones.

e) Simple Formula [15, 16]

$$q_{gw} = \frac{5.1564 \cdot 10^{-5}}{\sqrt{R_N}} \rho_\infty^{0.5} v_\infty^{3.15}. \qquad (10.76)$$

The input dimensions, as also for the other relations, are kg/m^3 for the density ρ_∞ and m/s for the flight speed v_∞. The resulting q_{gw} has the dimension W/m^2.

This relation is a correlation of data from several sources, based on eq. (2.5). This is a rapid and fair approximation of the heat flux in the gas at the wall at the stagnation point of a sphere. It serves typically in trajectory determination and optimization with the forward stagnation point as reference location, Chapter 2.

10.4 Flat Surface Boundary Layer Parameters Based on the Reference-Temperature/Enthalpy Concept

The reference-temperature/enthalpy concept permits the temperature and compressibility effects to be accounted for approximately and in a simple way to enable the determination of boundary layer parameters [17]. When used as the reference-enthalpy concept, it enables high enthalpy flows to be treated [18]. The reference-temperature/enthalpy concept is discussed in some detail in [1]. It is not an exact but a well-proven approximate concept. Basically it works with boundary layer relations established for incompressible flow. These are applied with the inviscid flow data at the body surface, which are interpreted as being those at the boundary layer edge. Density and viscosity are interpreted as function of an appropriate reference temperature or enthalpy. In [19], for instance, the viability of the approach is demonstrated. Generalized formulations, which are valid for attached laminar and turbulent flow can be found in [20].

10.4.1 Reference-Temperature/Enthalpy Concept

The characteristic Reynolds number for a high-speed boundary-layer like flow is postulated to read

$$Re_x^* = \frac{\rho^* v_e x}{\mu^*}. \qquad (10.77)$$

Density ρ^* and viscosity μ^* are reference data, characteristic of the boundary layer. They are determined with the local pressure p and the reference enthalpy h^* or with the reference temperature T^*, with v_e the external inviscid flow velocity. The reference temperature T^* is empirically composed of the boundary layer edge temperature T_e (without hypersonic viscous interaction identical to T_∞), the wall temperature T_w, and the recovery temperature T_r [17]

$$T^* = 0.28T_e + 0.5T_w + 0.22T_r. \tag{10.78}$$

The general reference enthalpy h^* is defined similarly [18]

$$h^* = 0.28h_e + 0.5h_w + 0.22h_r. \tag{10.79}$$

The recovery data are found with

$$T_r = T_e + r^* \frac{v_e^2}{2c_p}, \tag{10.80}$$

or

$$h_r = h_e + r_h^* \frac{v_e^2}{2}. \tag{10.81}$$

Here r^* or r_h^* is the recovery factor, which is a function of the Prandtl number Pr. The Prandtl number depends rather weakly on the temperature, or the enthalpy, up to $T \approx 5,000$ K. Usually it is sufficient to assume $r^* = r = $ const. For laminar flow the recovery factor is $r = \sqrt{Pr}$, and for turbulent flow $r = \sqrt[3]{Pr}$. With the Prandtl number at low temperatures, $Pr \approx 0.74$ [1], we get $r_{lam} \approx 0.86$ and $r_{turb} \approx 0.90$.

Introducing the boundary layer edge data as reference flow data into eq. (10.77) yields

$$Re_x^* = \frac{\rho_e v_e x}{\mu_e} \frac{\rho^*}{\rho_e} \frac{\mu_e}{\mu^*} = Re_{e,x} \frac{\rho^*}{\rho_e} \frac{\mu_e}{\mu^*}, \tag{10.82}$$

with $Re_{e,x} = \rho_e v_e x/\mu_e$. This relation can be simplified. If we apply it to boundary layer like flows, we can write, because $p = p_e = p_w$

$$\frac{\rho^*}{\rho_e} = \frac{T_e}{T^*}. \tag{10.83}$$

If, for simplicity, we further assume a power-law expression for the viscosity, we obtain

$$\frac{\mu^*}{\mu_e} = \frac{(T^*)^{\omega^*}}{(T_e)^{\omega_e}}. \tag{10.84}$$

Only if T^* and T_e are both in the same temperature interval, ω^* and ω_e are equal [1] and we get:

$$\frac{\mu^*}{\mu_e} = \left(\frac{T^*}{T_e}\right)^\omega. \tag{10.85}$$

Introducing eqs. (10.83) and (10.85) into eq. (10.82) reduces the latter to

$$Re_x^* = Re_{e,x} \left(\frac{T_e}{T^*}\right)^{1+\omega}. \tag{10.86}$$

10.4.2 Boundary Layer Thicknesses Over Flat Surfaces

In this and the following sub-sections we give the flat-plate relations in generalized form [20]; see also [1]. The exponent in the following relations is $n = 0.5$ for laminar and $n = 0.2$ for turbulent flow. If T^* and T_e are both in the same temperature interval (see above), the exponents ω^* and ω_e are equal, and the given relations can be further reduced. The boundary layer thickness δ reads

$$\delta = C \frac{x}{(Re_{e,x}^*)^n}, \tag{10.87}$$

with $C = 5$ for laminar and $C = 0.37$ for turbulent flow.

Specializing for the reference temperature, we obtain with $Re^u = \rho_e \, v_e / \mu_e$

$$\delta = C \frac{x^{1-n}}{(Re_e^u)^n} \left(\frac{\rho_e \, \mu^*}{\rho^* \, \mu_e} \right)^n. \tag{10.88}$$

An alternative formulation for the thickness of laminar compressible boundary layers is [21]

$$\delta_{lam} = x^{0.5} \sqrt{\frac{C^*}{Re_e^u}} \left(5 + 2.21 \frac{\gamma - 1}{2} M_\infty^2 + 1.93 \frac{T_w - T_r}{T_e} \right), \tag{10.89}$$

with

$$C^* = \frac{\mu^* T_e}{\mu_e T^*}. \tag{10.90}$$

The relations for the displacement thickness δ_1 are similar. For the laminar case we have

$$\delta_{1,lam} = \delta_{1,lam,ic} \left(-0.122 + 1.122 \frac{T_w}{T_\infty} + \right.$$
$$\left. + 0.333 \frac{\gamma_\infty - 1}{2} M_\infty^2 \right) \left(\frac{T^*}{T_\infty} \right)^{0.5(\omega - 1)}, \tag{10.91}$$

with that for laminar incompressible flow being

$$\delta_{1,lam,ic} = 1.7208 \frac{x}{(Re_{\infty,x})^{0.5}}. \tag{10.92}$$

For turbulent flow the relation reads

$$\delta_{1,turb,c} = \delta_{1,turb,ic} \left(0.129 + 0.871 \frac{T_w}{T_\infty} + \right.$$
$$\left. + 0.648 \frac{\gamma_\infty - 1}{2} M_\infty^2 \right) \left(\frac{T^*}{T_\infty} \right)^{0.2(\omega - 4)}, \tag{10.93}$$

with that for turbulent incompressible flow

$$\delta_{1,turb,ic} = 0.0504 \frac{x}{(Re_{\infty,x})^{0.2}}. \tag{10.94}$$

The relation for the momentum thickness δ_2 is

$$\delta_2 = C_2 \frac{x^{1-n}}{1-n} \left(\frac{\rho^* \mu^*}{\rho_e \mu_e}\right)^n \left(\frac{\rho^*}{\rho_e}\right)^{1-2n} \left(\frac{1}{Re_e^u}\right)^n, \tag{10.95}$$

with $C_2 = 0.332$ for laminar flow and $C_2 = 0.0296$ for turbulent flow.
For the thickness of the viscous sub-layer we have

$$\delta_{vs} = 29.06 \frac{x^{0.1}}{(Re_e^u)^{0.9}} \left(\frac{\rho_e}{\rho^*} \frac{\mu^*}{\mu_e}\right)^{0.9}, \tag{10.96}$$

whereas the turbulent scaling thickness reads

$$\delta_{vs} = 33.78 \frac{x^{0.2}}{(Re_e^u)^{0.8}} \left(\frac{\rho_e}{\rho^*} \frac{\mu^*}{\mu_e}\right)^{0.8}. \tag{10.97}$$

10.4.3 Wall Shear Stress and Thermal State at Flat Surfaces

For the wall shear stress over a flat plate we get in generalized form, with $C = 0.332$ for laminar flow and $C = 0.0296$ for turbulent flow

$$\tau_w = C\mu_e v_e x^{-n} \left(\frac{T_e}{T^*}\right)^{1-n} \left(\frac{\mu^*}{\mu_e}\right)^n (Re_e^u)^{1-n}. \tag{10.98}$$

This can also be written as

$$\frac{\tau_w}{0.5\rho_e v_e^2} = c_f = 2Cx^{-n} \left(\frac{T_e}{T^*}\right)^{1-n} \left(\frac{\mu^*}{\mu_e}\right)^n (Re_e^u)^{-n}. \tag{10.99}$$

The heat flux in the gas at the wall reads, again with $C = 0.332$ for laminar flow and $C = 0.0296$ for turbulent flow

$$q_{gw} = Cx^{-n} k_e Pr^{1/3}(T_r - T_w) \left(\frac{T_e}{T^*}\right)^{1-n} \left(\frac{\mu^*}{\mu_e}\right)^n (Re_e^u)^{1-n}. \tag{10.100}$$

The (implicit) relation for the radiation-adiabatic wall temperature is

$$T_{ra} = \left[Cx^{-n} \frac{k_e}{\sigma\varepsilon} Pr^{1/3}(T_r - T_{ra}) \left(\frac{T_e}{T^*}\right)^{1-n} \left(\frac{\mu^*}{\mu_e}\right)^n (Re_e^u)^{1-n} \right]^{0.25}. \tag{10.101}$$
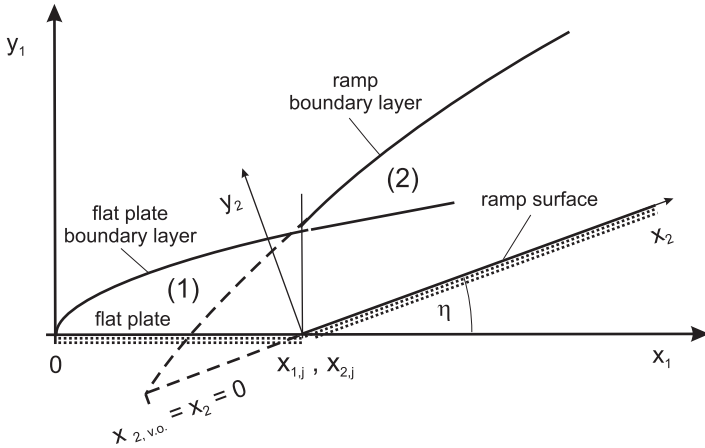
Fig. 10.4. Illustration of the virtual origin of a boundary layer at a junction demonstrated by means of a flat plate/ramp configuration.

10.4.4 Virtual Origin of Boundary Layers at Junctions

If the simple relations provided above are to be applied on consecutive surfaces with a change of characteristic properties, a virtual origin at the junction(s) must be constructed.[9] We show this with the help of the flat-plate/ramp configuration given in Fig. 10.4. With a flat-plate flow Mach number $M_1 > 1$, we get at the junction of the two planar surfaces a jump of the flow parameters, and especially of the unit Reynolds number, Fig. 6.18, depending on the ramp angle η and on the flat-plate flow Mach number M_1. Of course, in the frame of the simple approach we cannot describe local strong interaction phenomena, only the asymptotic properties on the ramp, Section 6.3.

If Re^u changes at the junction, the boundary layer on the ramp surface (2), Fig. 10.4, has other properties than that on the flat plate (1). It cannot be assumed, that simply a continuation takes place. In [22] therefore a matching procedure is proposed, which essentially leads to a ramp boundary layer with a virtual origin different from that of the flat plate.

Proposed in [22] is the matching of the momentum deficit of the two boundary layers on both sides of the junction $x_{1,j} = x_{2,j}$

$$(\rho u^2 \delta_2)|_2 = (\rho u^2 \delta_2)|_1, \tag{10.102}$$

with δ_2 being the momentum-loss thickness, see above.

The procedure is the following:

– determine $\delta_2|_1$, eq. (10.95), at the junction $x_1 = x_{1,j}$ with the flow parameters of the flat plate (1),

---

[9]   This holds, for instance, also for the correlation of experimental data.

– determine $\delta_2|_2$ from eq. (10.102) with the ramp flow parameters (2),
– find the virtual junction coordinate $x_{2,j}$ of the ramp boundary layer with the inverted eq. (10.95). The effective ramp coordinate is then in terms of x_1 and the ramp angle η: $x_2 = x_{2,j} + (x_1 - x_{1,j})/\cos\eta$. The virtual origin $x_{2,vo}$ of the ramp boundary layer lies at $x_2 = -x_{2,j}$.

This approach, in analogous ways, can be applied to cone/cylinder, blunt-nose/cylinder and other configurations [22, 23, 20], including laminar-turbulent transition, for instance on a flat surface, where the prescribed transition point would be the junction point. When employing discrete numerical methods for the solution of the boundary layer or the Navier–Stokes equations for the flow past such configurations, of course such an approach is not necessary.

References

1. Hirschel, E.H.: Basics of Aerothermodynamics. Progress in Astronautics and Aeronautics, AIAA, Reston, Va, vol. 204. Springer, Heidelberg (2004)
2. Adams, J.C., Martindale, W.R., Mayne, A.W., Marchand, E.O.: Real Gas Scale Effects on Hypersonic Laminar Boundary-layer Parameters Including Effects of Entropy-Layer Swallowing. AIAA-Paper 76-358 (1976)
3. Schwane, R., Muylaert, J.: Design of the Validation Experiment Hyperboloid-Flare. ESA Doc. YPA/1256/RS, ESTEC (1992)
4. Wüthrich, S., Sawley, M.L., Perruchoud, G.: The Coupled Euler/ Boundary-Layer Method as a Design Tool for Hypersonic Re-Entry Vehicles. Zeitschrift für Flugwissenschaften und Weltraumforschung (ZFW) 20(3), 137–144 (1996)
5. Brauckmann, G.J., Paulson Jr., J.W., Weilmuenster, K.J.: Experimental and Computational Analysis of Shuttle Orbiter Hypersonic Trim Anomaly. Journal of Spacecraft and Rockets 32(5), 758–764 (1995)
6. Ames Research Staff. Equations, Tables, and Charts for Compressible Flow. NACA R-1135 (1953)
7. Vincenti, W.G., Kruger, C.H.: Introduction to Physical Gas Dynamics. John Wiley, New York (1965); Reprint edition, Krieger Publishing Comp., Melbourne, Fl. (1975)
8. Paulson Jr., J.W., Brauckmann, G.J.: Recent Ground-Facility Simulations of Space Shuttle Orbiter Aerodynamics. In: Throckmorton, D.A. (ed.), Orbiter Experiments (OEX) Aerothermodynamics Symposium. NASA CP-3248, Part 1, pp. 411–445 (1995)
9. Van Driest, E.R.: On Skin Friction and Heat Transfer Near the Stagnation Point. NACA Report, AL-2267 (1956)
10. Lees, L.: Laminar Heat Transfer over Blunt-Nosed Bodies at Hypersonic Flight Speeds. Jet Propulsion 26(4), 259–269 (1956)
11. Bertin, J.J.: The Effect of Protuberances, Cavities, and Angle of Attack on the Wind Tunnel Pressure and Heat Transfer Distribution for the Apollo Command Module. NASA TM X-1243 (1966)
12. Fay, J.A., Riddell, F.R.: Theory of Stagnation Point Heat Transfer in Dissociated Air. Journal of Aeronautical Sciences 25(2), 73–85 (1958)

13. Cohen, N.B.: Boundary Layer Similar Solutions and Correlation Equations for Laminar Heat Transfer Distribution in Equilibrium Air at Velocities Up to 41,100 Feet Per Second. NASA TR R-118 (1961)
14. Zoby, E.V., Moss, J.N., Sutton, K.: Approximate Convective Heating Equations for Hypersonic Flows. Journal of Spacecraft 18(1) (1981)
15. Detra, R.W., Kemp, N.H., Riddell, F.R.: Addendum to Heat Transfer to Satellite Vehicles Reentering the Atmosphere. Jet Propulsion 27(12), 1256–1257 (1957)
16. Riley, C.J., DeJearnette, F.R.: Engineering Aerodynamic Heating Method for Hypersonic Flow. Journal of Spacecraft and Rockets 29(3) (1992)
17. Rubesin, M.W., Johnson, H.A.: A Critical Review of Skin Friction and Heat Transfer Solutions of the Laminar Boundary Layer of a Flat Plate. Trans. ASME 71, 385–388 (1949)
18. Eckert, E.R.G.: Engineering Relations of Friction and Heat Transfer to Surfaces in High-Velocity Flow. J. Aeronautical Sciences 22(8), 585–587 (1955)
19. Simeonides, G., Walpot, L.M.G., Netterfield, M., Tumino, G.: Evaluation of Engineering Heat Transfer Prediction Methods in High Enthalpy Flow Conditions. AIAA-Paper 96-1860 (1996)
20. Simeonides, G.: Generalized Reference-Enthalpy Formulation and Simulation of Viscous Effects in Hypersonic Flow. Shock Waves 8(3), 161–172 (1998)
21. Simeonides, G.: Hypersonic Shock Wave Boundary Layer Interactions over Compression Corners. Doctoral Thesis, University of Bristol, U.K (1992)
22. Hayes, J.R., Neumann, R.D.: Introduction to the Aerodynamic Heating Analysis of Supersonic Missiles. In: Mendenhall, M. R. (ed.), Tactical Missile Aerodynamics: Prediction Methodology. Progress in Astronautics and Aeronautics, AIAA, Reston, Va, pp. 63–110 (1992)
23. Streit, T., Martin, S., Eggers, T.: Approximate Heat Transfer Methods for Hypersonic Flow in Comparison with Results Provided by Numerical Navier-Stokes Solutions. DLR FB 94-36 (1994)